Modelling, Simulation and Hardware-in-the-Loop Validation of Virtual Synchronous Generator Control in Low Inertia Power System

Junru Chen, Muyang Liu, Cathal O'Loughlin, Federico Milano, Terence O'Donnell
University College Dublin
Dublin, Ireland
Junru.chen.1@ucdconnect.ie

***Abstract*— In recent literature, virtual synchronous generator control (VSG) has been proposed as a means to provide virtual inertia from non-synchronous generation in low inertia power systems. In this work we compare the power system support performance of VSG control to conventional droop when applied to electrical energy storage. A differential-algebraic equations (DAEs) model of VSG control is developed. This model is validated against measurement from a hardware in the loop implementation of the VSG. VSG and droop controlled storage is then incorporated into the IEEE 39 bus system model also incorporating different levels of generation from windfarms. The performance of both controls is compared in terms of their effect on the power system dynamics in the event of a contingency. The results show that VSG control in high wind penetration cases, improves the frequency nadir, reduces oscillations, and provide faster frequency and voltage stabilization.**

***Index Terms*—virtual synchronous generator, VSG modelling, droop control, N-1 contingency.**

I. INTRODUCTION

The increase in renewable generation from solar plants and wind farms reduces the inertia of the power system, with potential impacts for the system stability. In order to greatly increase the use of renewables while maintaining system stability, these power electronics connected generation sources must move from being purely grid feeding to grid supporting and potentially grid forming. It is therefore important to implement control approaches which can work well as grid support in an synchronous generator (SG) dominated system, while also maintaining stability in a non-synchronous generation dominated grid. One such control techniques is virtual synchronous generator (VSG) control, which has been proposed to provide frequency support by emulating the inertia in the control of grid connected converters [1].

Much work has already been done on the different implementation approaches of VSG control, including, development of small signal models [2]-[5], investigations of the different topologies [2]-[7] when connected to different power sources [7], and analysis of its behavior in microgrids and standalone systems [8]. Although there has been considerable analysis of the use of VSG control in microgrids, the analysis of VSG behavior in a more conventional power system is still lacking. On the other hand, virtual inertia control has been well researched in conventional power systems. References [9]-[12] present the implementation of virtual inertia control for double fed induction generator (DFIG) in terms of both modelling and case studies, including the emulation of inertia from the DFIG rotating mass, from energy storage systems (ESS), and from super-capacitor storage. In addition [13] had applied virtual inertia control to PV systems with analysis in a 6-bus power system model. However, inertia emulation is only a part of VSG control. In addition to virtual inertia, the VSG control can include virtual impedance and reactive power voltage droop. The potential purpose of VSG is not only as an auxiliary control to support the grid frequency but as a main control to forming the grid frequency in a manner similar to synchronous machines. Thus, it does not require a Phase Lock Loop (PLL) to stay synchronized as it relies on an emulation of the swing equation to automatically and dynamically vary its angle and potential.

From the perspective of provision of voltage and frequency support, it is well understood that these can be provided in the power system by incorporating ESS with droop control. Indeed the dynamic performances of VSG and droop controls have previously been compared for distributed generation [14], however only for the case of a single VSG connected to a single generator.

Although previous works [2]-[5] and [15] have established the model of the VSG based on nonlinear differential-algebraic equations (DAEs), ordinary differential equations (ODEs), and linear small signal models, none of these works have integrated the VSG model with the conventional power system model. The contribution of this work is to provide such a model and to compare the dynamic response of the proposed VSG control and conventional droop control for frequency and voltage support from ESS. The VSG control in ESS is expected to have better support performance than the droop control, due to its inertial emulation. Hence we focus on a comparison of the performance from the power system dynamics perspective, especially the low inertia system. The controls are implemented on ESS, co-located with windfarms

This work is part of Energy Systems Integration Partnership Programme (ESIPP) Project funded by the Science Foundation Ireland (SFI) Strategic Partnership Programme Grant Number SFI/15/SPP/E3125.

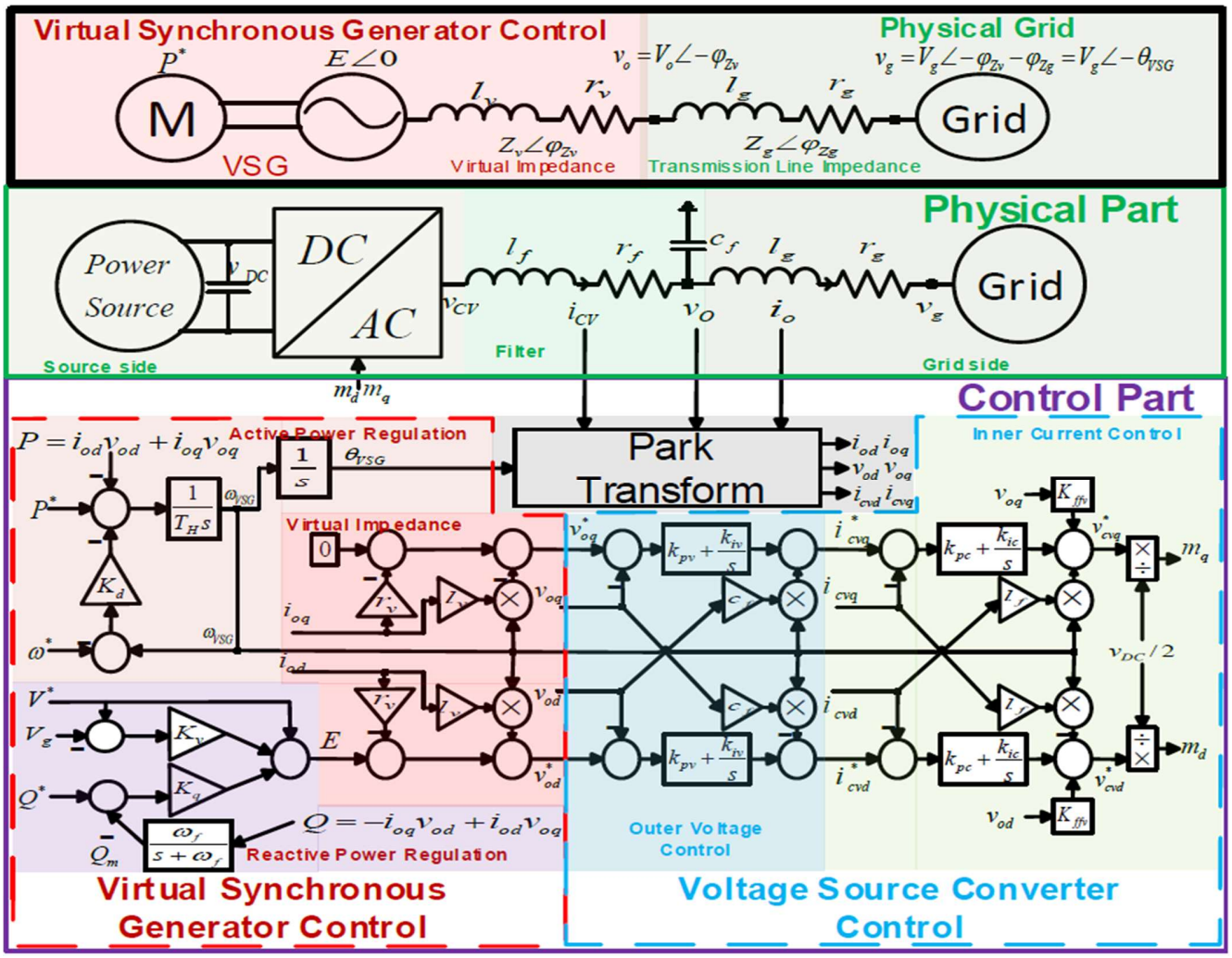

Figure 1. Virtual Synchronous Generator

and stability is investigated as the penetration of generation from wind is increased.

The paper is organized as follows: Section II reviews the VSG nonlinear DAE model, and verifies the model in a comparison with experimental results from hardware. Section III compares the performance of VSG control to droop control using as a case study the stability of the IEEE 39 bus system with wind generation under N-1 contingency conditions.

II. Virtual Synchronous Generator Modelling

This work is based on the widely used power forming or voltage source type VSG [3-6,20]. The VSG control consists of two parts. The first part is the actual synchronous machine emulation, including the emulation of the swing equation dynamics, real power to voltage angle regulation, reactive power to voltage droop and a virtual impedance. The second part consists of the voltage source converter (VSC) controls (outer voltage, inner current dq frame controllers) which receives the references from the first part. The entire system is shown in Fig. 1. Below we review each part of VSG and provide its corresponding model equations. Since the aim of this work is primarily to investigate the system level advantages of using VSG control. To simplify the analysis, the model is built under the assumption of replacing the storage by an ideal DC voltage source with infinite capacity and fast response, and unlimited converter power transfer.

A. Virtual Synchronous Generator Control Part

The core function of VSG control is to regulate the angle difference between the electric potential E and grid voltage V_g according to the active power-angle swing equation, and the magnitude of the electric potential E according to the reactive power-voltage droop. Thus, the power flow into the grid is controlled.

1) Swing Equation

The swing equation applied in VSG contains three parts as indicated in (1): inertia emulation T_H ,active power droop P_{droop} and the active power difference between the reference and real output active power, where, the reference power mimics the mechanical input power, of a synchronous machine. In a synchronous machine model, a damping term is also present which is proportional to the difference between machine frequency and grid frequency whereas the droop is the difference between the grid frequency and the nominal frequency. In VSG, the gain K_D for the droop and the damping can be set to be the same value, thus the droop (4) can be

directly embedded into (1). The VSG droop gain K_D therefore implements both droop and damping features. The equations describing the VSG transient behavior are given below.

$$T_H \frac{d\,\Delta\,\omega_{VSG}}{dt} = P^* + P_{droop} - P \quad (1)$$

$$\Delta\omega_{VSG} = \omega_{VSG} - \omega_{grid} \quad (2)$$

$$\frac{d\theta_{VSG}}{dt} = \Delta\omega_{VSG}\omega_{base} \quad (3)$$

$$P_{droop} = K_D(\omega^* - \omega_{VSG}) \quad (4)$$

$$P = i_{od}v_{od} + i_{oq}v_{oq} \quad (5)$$

where K_D is the droop/damping gain, P^* is the reference active power, P is VSG output active power, ω^* is the nominal frequency, ω_{base} is the base frequency, ω_{VSG} is the VSG frequency (dq-frame rotating speed in VSC), ω_{grid} is the grid frequency, v_{od}/v_{oq} is the VSG output voltage in dq-frame, i_{od}/i_{oq} is the VSG output current in dq-frame.

2) Reactive Power-Voltage Droop

As will be seen later, there is a coupling between the active and reactive power control in the VSG. Here we investigate the use of two different voltage - reactive power controls. Both are described by (6) where either the emulated electric potential E is drooped by reactive power as described by (7a) with gain K_q or by voltage as described by (7b) with gain K_v [20]. V^* is the nominal voltage, and the reactive power used in the droop relationship Q_m is the actual reactive power, Q, passed through a low pass-filter with corner frequency, ω_f as described by (8). Q^* is the reference reactive power.

$$E = V^* + \Delta V_{droop} + \Delta V_{comp} \quad (6)$$

$$\Delta V_{droop} = K_q(Q^* - Q_m) \quad (7a)$$

$$\Delta V_{comp} = K_v\left(V^* - V_g\right) \quad (7b)$$

$$\frac{dQ_m}{dt} = -\omega_f Q_m + \omega_f Q \quad (8)$$

$$Q = -i_{oq}v_{od} + i_{od}v_{oq} \quad (9)$$

Note only one of K_v or K_q is non-zero for either control. With K_q non-zero (K_v zero) ΔV_{droop} aims to provide reactive power sharing, while K_v non-zero (K_q zero) ΔV_{comp} aims to provide reactive power to support the grid voltage.

3) Virtual Impedance

A virtual impedance (including virtual inductance l_v and resistance r_v), which is used to modify power sharing for different line impedances, can be emulated by the controller. By feedback of the output current into the virtual impedance algorithm, the voltage drop across the virtual impedance which exists between the electric potential E and the computed output voltage reference (10) can be emulated. Assuming a fast enough VSC response the output voltage can be considered to follow its reference instantaneously, so that the virtual impedance behaves like a real impedance in series with the transmission line impedance as shown in the top of Fig. 1. E is set as the reference phase angle (0 rad).

$$v_{od}^* = E + \omega_{VSG}l_v i_{oq} - r_v\, i_{od} \quad (10a)$$

$$v_{oq}^* = -r_v i_{oq} - \omega_{VSG}l_v i_{od} \quad (10b)$$

where $i_o = i_{od} + ji_{oq}$ is output current, $v_o^* = v_{od}^* + jv_{od=}^*$ is the reference voltage to VSC controller.

The virtual synchronous generator control provides the reference voltage to the VSC control. Note also that the reference frame for the dq transform is aligned with the VSG rotation.

B. Voltage Source Converter Control

The VSC voltage controller regulates the output voltage at the point of common coupling to the grid. The outer voltage controller generates a reference for the inner current controller, which in turn determines the VCS terminal voltage v_{cv}. The details of the standard VSC outer voltage-inner current control which ensures that the output voltage follows its reference is well covered in many previous works such as reference [16] so that only the main equations are presented here.

1) Voltage Controller

The reference for the inner current controller, i_{cv}^* is computed by the voltage controller with a PI controller K_{pv}, K_{iv} as indicated in (11). ε is the integral of the voltage error as given by (12).

$$i_{cvd}^* = K_{pv}(v_{od}^* - v_{od}) + K_{iv}\varepsilon_d - \omega_{VSG}c_f v_{oq} \quad (11a)$$

$$i_{cvq}^* = K_{pv}\left(v_{oq}^* - v_{oq}\right) + K_{iv}\varepsilon_q + \omega_{VSG}c_f v_{od} \quad (11b)$$

$$\frac{d\varepsilon_d}{dt} = v_{od}^* - v_{od} \quad (12a)$$

$$\frac{d\varepsilon_q}{dt} = v_{oq}^* - v_{oq} \quad (12b)$$

2) Current Controller

The terminal voltage v_{cv}^* can be computed by the current controller with PI controller K_{pc}, K_{ic} and feedforward voltage compensator K_{ffv} in (13). γ is the integral of the current error as given by (14).

$$v_{cvd}^* = K_{pc}(i_{cvd}^* - i_{cvd}) + K_{ic}\gamma_d - \omega_{VSG}l_f i_{cvq} + K_{ffv}v_{od} \quad (13a)$$

$$v_{cvq}^* = K_{pc}\left(i_{cvq}^* - i_{cvq}\right) + K_{ic}\gamma_q + \omega_{VSG}l_f i_{cvd} + K_{ffv}v_{oq} \quad (13b)$$

$$\frac{d\gamma_d}{dt} = i_{cvd}^* - i_{cvd} \quad (14a)$$

$$\frac{d\gamma_q}{dt} = i_{cvq}^* - i_{cvq} \quad (14b)$$

C. Electric Circuit Model

The circuit equations account for the voltage drop on filter inductor (15), the current flow into filter capacitor (16) and the voltage drop on the transmission line (17). As the electric potential, E, is taken as the reference, the phase angle of grid voltage V_g (in amplitude) is $-\theta_{VSG}$.

$$\frac{l_f}{\omega_{base}}\frac{di_{cvd}}{dt} = v_{cvd} - v_{od} - r_f i_{cvd} + \omega_{grid}l_f i_{cvq} \quad (15a)$$

$$\frac{l_f}{\omega_{base}}\frac{di_{cvq}}{dt} = v_{cvq} - v_{oq} - r_f i_{cvq} - \omega_{grid}l_f i_{cvd} \quad (15b)$$

$$\frac{c_f}{\omega_{base}}\frac{dv_{od}}{dt} = i_{cvd} - i_{od} + \omega_{grid}c_f v_{oq} \quad (16a)$$

$$\frac{c_f}{\omega_{base}}\frac{dv_{oq}}{dt} = i_{cvq} - i_{oq} - \omega_{grid}c_f v_{od} \quad (16b)$$

$$\frac{l_g}{\omega_{base}}\frac{di_{od}}{dt} = v_{od} - V_g\cos(-\theta_{VSG}) - r_g i_{od} + \omega_{grid}l_g i_{oq} \quad (17a)$$

$$\frac{l_g}{\omega_{base}}\frac{di_{oq}}{dt} = v_{oq} - V_g\sin(-\theta_{VSG}) - r_g i_{oq} - \omega_{grid}l_g i_{od} \quad (17b)$$

Equation (1)-(17) represent the complete DAE model of the VSG.

D. Model Validation

The DAE model has been validated using a comparison with experimental results obtained from hardware in the loop measurements with the same settings. The hardware consists of two 100 V, 2 kVA three-phase AC/DC converters interfaced with an OPAL-RT real time simulation platform. One of these converters implements the VSG control, while the other converter emulates the grid with adjustable voltage and frequency. The transmission line impedance is modelled as a series impedance. Parameters and system settings are summarized in Table I. The DAE model for comparison is run in Matlab/Simulink.

For the hardware tests, besides the fixed input v_g, V^* and ω^* in Table I, P^* is step changed from 0 W to 500 W at 2.5 s, Q^* is step changed from 0 VA to 500 VA at 12.5 s and ω_{grid} is step changed from 50 Hz to 49.9 Hz at 22.5 s. Correspondingly, the DAE model experiences the same changes.

Fig. 2 depicts the results from the hardware experiment (blue line) and compares it with the result from the DAE model (red line). In total, the DAE closely matches the hardware experiment result, expect that the hardware results show some resonance effects during transients which is due to the VSC harmonic impedance interactions. Meanwhile, both these results reveal some defects of the VSG control as implemented here. Firstly, it can be seen that the VSG only tracks active power reference accurately while it has a significant steady state error on reactive power tracking in the reactive power sharing control (this is because that it is impossible for the V^* and Q^* to be satisfied at the same time when the $\Delta V_{comp} = 0$ in (6)), and secondly, the active power and reactive power are coupled. These are due to the fact that the VSG emulates the SG and controls the electric potential and angle as opposed to the decoupled d and q axis currents as in conventional droop control.

TABLE I
HARDWARE VSG SETTINGS

Parameter	Value	Parameter	Value
PWM/Sampling time	1350/ 14.81e-6 s	Filter inductance	0.033 H
Rated Voltage $\widehat{v_g}$	100 V	Filter resistance	0.1266 Ω
Reference voltage V^*	100 V	Filter capacitance	80 μF
Reference angular frequency ω^*	2π*50 Hz	Line inductance	0.033 H
VSG Inertia T_H	50 W/(rad·s^{-2})	Line resistance	1.44 Ω
damping/droop K_D	400 W/(rad·s^{-1})	Virtual inductance	0.0037 H
reactive power droop K_q	0.01 V/VA	Virtual resistance	0.01 Ω
Current controller P/I	66/339.8	Voltage controller P/I	0.0535/ 11.987

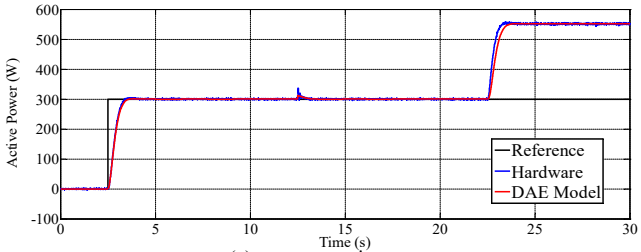

(a) output active power

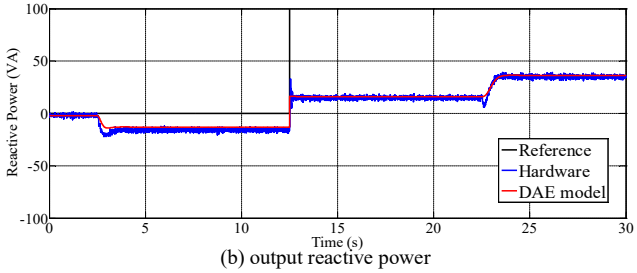

(b) output reactive power

Fig. 2. Comparison results on hardware and DAE model

III. DROOP CONTROL

In previous works, it has been shown that the virtual inertia in VSGs can help reduce the rate of change of the frequency (RoCoF), while droop control provides support for steady state frequency deviations. The kernel of this paper is to implement VSG into the conventional system and compare its behavior with presently used droop control in ESS. In this section, the paper reviews the ESS with droop control and highlights the difference between the droop control and VSG control.

In the proposed VSG model, the DC side is assumed to be an ideal DC source and the same assumption is applied to the droop control. The commonly used (*f-P, V-Q*) droop control [22] is based on the current controlled VSC i.e. grid frequency to active power droop (18) and voltage to reactive power droop (19). The current obtained from (18) and (19) is the reference dq-frame current in the inner current control in Fig. 1.

$$i_{cvd}^* = (P^* + K_D(\omega^* - \omega_{pll}))/V_g \tag{18}$$

$$i_{cvq}^* = (Q^* + \frac{1}{K_q}(V^* - V_g))/V_g \tag{19}$$

where K_D is the frequency to active power droop gain and corresponds to that in VSG, K_q is the voltage to reactive power droop gain and corresponds to that in VSG. ω_{pll} is the grid frequency as measured by a PLL [21]. Note that, in the ESS with droop control, only L filter may be required, thus, i_{cv} equals to i_o. Then, the complete ideal droop controlled VSC equations, consist of (18),(19), as well as SRF-PLL equations in [21], plus the current controller (13), electric circuit equation (15), and power computation (5),(9).

The droop control applies outer power, inner current control, thus, the control outputs are power. However, VSG control applies outer voltage inner current control, so that its control outputs are voltage amplitude and angle. In VSG control, both voltage amplitude and angle affects the active power and reactive power output. Thus, the angle to active power control loop interacts with the amplitude to reactive power control loop. This couples the reactive power control with the active power control. In contrast, the droop control decouples active power and reactive power by separately regulating P by i_d (18) and Q by i_q (19). However, due to lack of inertia, the droop control behaves as a frequency and voltage follower. In addition, droop control relies on a

PLL to obtain the grid frequency and achieve synchronization, while the VSG determines its own frequency which self-synchronizes to the grid.

IV. Case Study

The purpose of this case study is to investigate the VSG control performance in a conventional system and compare it with presently used techniques (ESS embedded with droop control). The case studies are based on the New England 39-bus system (see Fig. 3) with 3 wind generators (WG) (37.2% wind penetration (WP)) or 8 WGs (87.6% WP) replacing synchronous generators. The SGs in the power system are modelled by 4th-order (two-axes) synchronous machine models. Each of the generators has both primary voltage (AVR and PSS) and frequency regulators (turbine governor). The WGs are modelled as variable-speed wind turbines with 5th-order doubly-fed induction machine models working at constant 13 m/s wind speed. For the ESS devices, in the VSG connected PV bus, the initial active power is set to zero. The frequency fed to the ESS is from the COI frequency [18] of the power system.

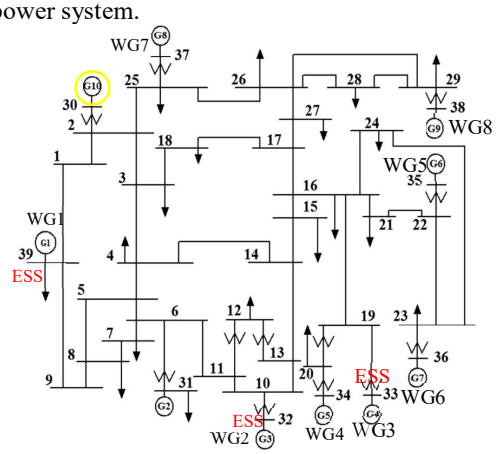

Figure 3: New England 39-bus system

In order to compare the VSG and droop control, we select the settings according to the following rules: 1) both controls are applied assuming an ideal DC source; 2) the VSC settings, including PI control and filter are the same; 3) the active droop gain K_D in (18) and (4) as well as the reactive droop gain K_q are the same; 4) for the VSG virtual inertia is selected so that the active power output in response to a frequency is overdamped, e.g. similar to the hardware test in Fig. 2. It has been shown previously [1] that the output power of the VSG is oscillatory unless sufficient damping is introduced. Here the damping is actually provided by the droop term. Thus, ensuring an overdamped response restricts the value of emulated inertia, which may not be optimal selection, as the virtual inertia may be too small to largely affect RoCoF. All the settings are listed in Table II.

We present three scenarios. The first scenario aims to investigate the characteristics of a single device in response to system contingencies. The second scenario simulates a more realistic situation with three ESS in the system. The last scenario compares the control in high WP situation with eight WGs in the system. All of these scenarios consider as a contingency, the loss of one SG.

The dynamic data of the original 10-synchronous-generator power system can be found in [18]. The wind generators data are listed in Table III. Simulation results in this section are obtained using Dome, a Python-based power system software tool [19].

TABLE II
Power System VSG and **Droop** Settings

Parameter	Value	Parameter	Value	Parameter	Value
$\boldsymbol{S_{base}}$	**100 MVA**	$\boldsymbol{V_n}$	**220 kV**	K_{pv}	25
T_H	20 s	$\boldsymbol{x_f}$	**0.08 pu**	K_{iv}	5
$\boldsymbol{K_q}$	**0.01**	$\boldsymbol{r_f}$	**0.01 pu**	ω_f	20
$\boldsymbol{K_D}$	**400**	b_f	0.34 pu	x_v	0.02 pu
$\boldsymbol{K_{pc}}$	**20**	x_g	0.08 pu	r_v	0.01 pu
$\boldsymbol{K_{ic}}$	**10**	r_g	0.005 pu	K_{ffv}	0.0

TABLE III
Wind Generators

Wind generator	1	2	3	4	5	6	7	8
S_n [MW]	1100	720	750	590	720	620	606	900
n_{gen}	540	362	350	275	365	301	295	451
w_{max}[pu]	1.20	1.2	1.19	1.21	1.14	1.19	1.19	1.19

A. Scenario 1: 37.2% WP One ESS

In this scenario, we aim to test the VSG and droop-based ESS devices, and compare their performance. Thus, only one ESS is co-located with WG1 in the system at bus 39. At 1 s, Gen 10 is lost. $K_V = 0$ represents the use of the reactive power sharing control, while $K_q = 0$ voltage support control. Fig. 4 presents the bus-39 frequency, voltage, ESS active and reactive power output under both controls in ESS.

In Fig. 4 (d), the ESS has an initial reactive power output due to its connection to a PV bus, where its initial reactive power is determined from a system power flow analysis.

From Fig. 4 (a), both controls can help support the frequency, while VSG control presents a somewhat larger damping or less oscillation. However, the droop control is somewhat superior for voltage support, due to its decoupled

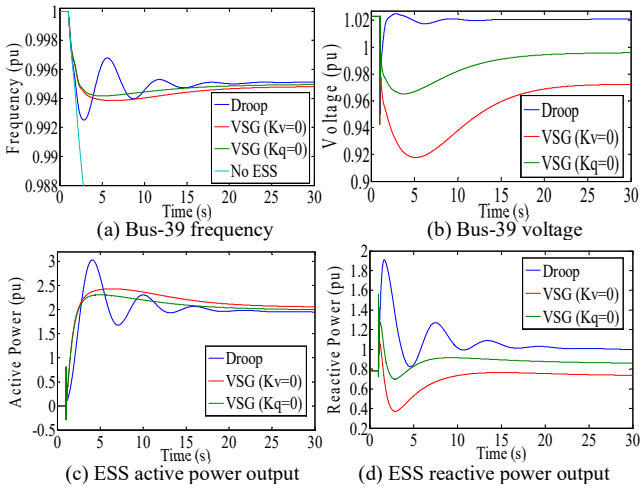

(a) Bus-39 frequency (b) Bus-39 voltage
(c) ESS active power output (d) ESS reactive power output

Figure 4: Scenario 2 results: 37.2% WP one ESS one SG lost.

reactive power. The VSG reactive power output experiences a dip in the initial 3 s owing to the active power increase, this can also be seen in the hardware test in Fig. 2 at 2.5 s. This initial insufficient reactive power support from the VSG results in a voltage decrease. Especially with the reactive powering sharing control of the VSG, the surge in output reactive power after the contingency at 1 s (due to the decrease in the bus voltage) results in the VSG potential decreasing in accordance with (6) and (7a) in an effort to track the reactive power reference (which equals to 0.8) as shown by the red line in Fig. 4 (d). This action further reduces the voltage at 5 s as indicated by the red line in Fig. 4 (b). On the other hand, due to the voltage dip after contingency, the voltage support control demands an increase in VSG electric potential in accordance with (6) and (7b). The action occurs simultaneously with the active power surge and results in less reactive power decrease and hence better compensation. The voltage transient performance is therefore better than that from the VSG with reactive power sharing control.

From the perspective of the ESS, Fig. 4 (c) and (d) show that although the VSG has less ability on reactive power compensation, the VSG control requires less ESS capacity than the droop control while still helping to stabilize the voltage in the standard range. Moreover, for the VSG, the emulated inertia affects both the active and reactive power output, leading to a smoother ESS discharge.

In this scenario however, it can be seen from the power graphs Fig. 4 (c) and (d), that the output (around 2.5 pu for active power and 1.2 pu for reactive power) is too large to be realistic and the VSG reactive power compensation problem is exaggerated. In a more realistic case, there may be more ESS distributed in the grid, with each ESS having a smaller capacity. In that case the reactive power could be compensated by the nearby ESS, and the power used to support frequency is shared by all the ESS. Considering the more realistic case, the reactive power compensation required from any one VSG would be less significant. Thus, the VSG control should have better performance on both frequency support and voltage support. This is investigated in the following scenario.

B. Scenario 2: 37.2% WP Three ESSs

In this scenario, three ESS devices are co-located with each WG at bus 39, 31 and 32 respectively. Two controls are compared under the same contingency as in scenario 2. Fig. 5 presents relevant results.

In this scenario, the drooped active power output is shared almost equally by the three ESS (see Fig. 4 (c) and Fig. 5 (c)). In comparison with Fig. 4 (a), increasing the number of ESS can improve the transient stability in both control (see Fig. 5 (a) from 0.992 pu to 0.995 pu for droop control and 0.994 pu to 0.998 pu for VSG control). However, the frequency in this case shows a small oscillation, which does not occur in the single ESS case. This is because the smaller active power output has less impact on reactive power output. Thus, the reactive power recovers faster in the three ESS case (compare Fig. 4 (d) and Fig. 5 (d)). The recovered reactive power peaks at around 3 s resulting in the frequency oscillation.

In this case, it can be seen that the VSG active-reactive coupling problem becomes insignificant as the number of ESS

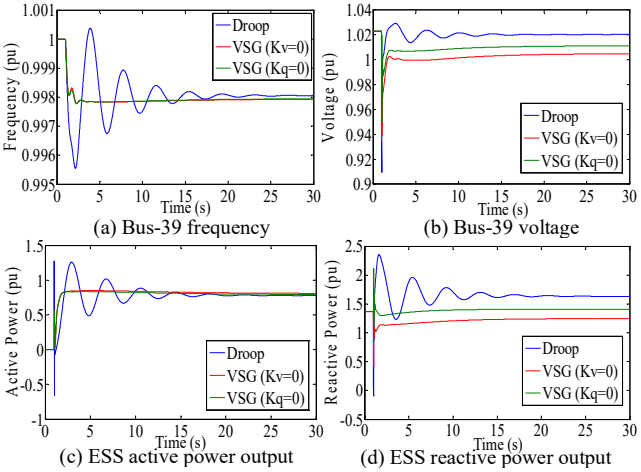

Figure 5: Scenario 2 results: 37.2% WP three ESS one SG lost.

are increased. Although the reactive power is still deficient, the voltage, compared with one ESS case, respond faster and is more stable. In addition, the gap between the VSG in reactive power sharing control and voltage support control is smaller. The three ESS with VSG control add a large virtual inertia to the system, thus, both frequency and voltage profiles show a strong damping under VSG control.

It should also be noted that, whatever the control, droop or VSG control, the frequency only changes by 0.005 pu (0.25 Hz) at maximum. This is because the system still has seven SGs online, which provide a significant inertia to the system. The following scenario investigates further the low inertia or high WP condition.

C. Scenario 3: 87.6% WP Three ESSs

In this scenario, eight SGs are replaced by WGs in the corresponding bus in the system as shown in Fig. 3. The ESS and contingency is the same as scenario 2. Fig. 6 presents the case results.

The inclusion of eight WGs leads to significantly reduce the system inertia. In comparison with Fig. 5 (a) , the droop control case has larger frequency oscillation after the

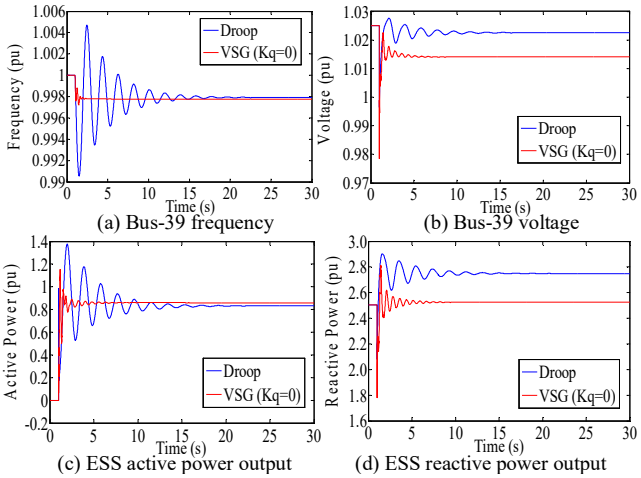

Figure 6: Scenario 2 results: 87.6% WP Three ESS one SG lost.

contingency as can be seen from Fig. 6 (a) (0.1 pu variation compared to 0.005 pu in scenario 2). However, for the VSG control, the frequency still only drops 0.02 pu at maximum. Moreover, the VSG control stabilizes the frequency in 3.5 s and the voltage in 7 s, while the droop control needs 20 s and 15 s respectively. The lower inertia in the system increases the oscillation in both cases. For the VSG control, although the virtual inertia also interacts in the electric potential control loop, the reactive power as well as voltage shows a high frequency oscillation after the contingency. This oscillation fades away in 7 s (due to virtual inertia), but it gives rise to the slight oscillation in the active power, and the initial frequency oscillation. This low inertia or high WP system, demonstrates the advantages of the VSG control over the droop control.

V. CONCLUSION

The paper presents and validates a VSG DAE model and its impact on the dynamic response of an interconnected power system. The paper also presents a comparison of the system stabilizing performance of VSG control and droop control applied to ESS. Based on the simulation results obtained using the discussed IEEE 39-bus system with WGs, we could draw the following conclusions:

1) The incorporation of ESS with either droop control or VSG control can improve system transient stability. In low wind penetration cases, the droop control has better voltage support, while, in high wind penetration cases, VSG control offers the possibility to improve the frequency nadir, reduce oscillations, and stabilize the frequency and voltage faster.

2) The control by which reactive power support is supplied by the VSG has important consequences for the voltage regulation. The reactive power sharing function (K_q) aims to track the reactive power reference, but worsens the voltage stability, while the voltage support (K_v) helps compensate the reactive power by tracking the voltage reference.

3) The main advantages of the VSG control is that implementation of virtual inertia can damp the frequency and power oscillation. However, the coupling of the real and reactive power controls can contribute to reduce voltage transient performance. However with an increased number of ESSs providing support, the VSG reactive power compensation problem becomes unimportant.

This work has several limitations which will be addressed in future work. Here in order to focus solely on the comparison of the control; the dynamics and limitations of the ESS have been neglected. In addition, in order to facilitate comparison the optimum choice of VSG and droop settings has not been investigated. For example, it is possible that increasing the VSG inertia term at the expense of increased oscillation may be beneficial in terms of reducing the RoCoF in the low inertia case.

REFERENCES

[1] H. Beck and R. Hesse, "Virtual Synchronous Machine," 2007 9th International Conference on Electrical Power Quality and Utilisation, pp.1-9, 2007.

[2] S. Arco, J. A. Suul and O. B. Fosso, "A Virtual Synchronous Machine implementation for distributed control of power converters in SmartGrids," Electric Power Systems Research, Vol. 122, pp. 180-197, May 2015.

[3] S. Acro, J. A. Suul and O. B. Fosso, "Small-signal modelling and parametric sensitivity of a Virtual Synchronous Machine", 2014 Power Systems Computation Conference (PSCC), Wroclaw, Poland, 18-22 Aug. 2014.

[4] S. Acro, J. A. Suul and O. B. Fosso, "Control system tuning and stability analysis of Virtual Synchronous Machines", 2013 Energy Conversion Congress and Exposition (ECCE), Denver, CO, USA, 15-19 Sept. 2013.

[5] O. Mo, S. Acro and J. Suul, "Evaluation of Virtual Synchronous Machines with Dynamic or Quasi-Stationary Machine Models", IEEE Transactions on Industrial Electronics, Vol. 64, no. 7, Jul. 2017.

[6] Q.-C. Zhong and G. Weiss, "Synchronverter: Inverters that mimic synchronous generators," IEEE Trans. In. Electron., vol. 58, no. 4, pp. 1259-1267, Apr. 2011.

[7] Q.-C. Zhong, P.-L. Nguyen, Z. Ma, and W. Sheng, "Self-synchronized synchronverters: Inverters without a dedicated synchronization unit," IEEE Trans. Power Electron., vol. 29, no. 2, pp. 617-630, Feb. 2014.

[8] S. D'Arco, and J. A. Suul, "Virtual Synchronous Machines - Classification of Implementations and Analysis of Equivalence to Droop Controllers for Microgrids", 2013 IEEE Grenoble PowerTech (POWERTECH), Grenoble, France, 16-20 June 2013, pp. 1-7,2013.

[9] M. F. M. Arani and E. EI-Saadany, "Implementing Virtual Inertia in DFIG-Based Wind Power Generation," IEEE Trans. Power Sys. Vol. 28, no. 2, May 2013.

[10] J. Ma, Z. Song, Y. Zhang, Y. Zhao and J. S. Thorp, "Robust Stochastic Stability Analysis Method of DFIG Integration on Power System Considering Virtual Inertia Control," IEEE Trans. Power Sys. Vol. 32, no. 5, Sep. 2017.

[11] M. F. M. Arani and E. F. EI-Saadany, "Incorporating DFIG based wind power generation in microgrid frequency regulation," 2012 Power and Energy Society General Meeting, San Diego, USA, 22-26 Jul. 2012.

[12] J. Ma, Y. Qiu, Y. Li, W. Zhang, Z. Song and J. S. Thorp, "Research on the Impact of DFIG Virtual Inertia Control on Power System Small-Signal Stability Considering the Phase-Locked Loop," IEEE Trans. Power Sys. Vol. 32, no. 3. May 2017.

[13] W. Im, C. Wang, W. Liu, L. Liu and J. Kim, "Distributed Virtual Inertia Based Control of Mutiple Photovoltaic Systems in Autonomous Microgrid," IEEE/CAA Journal of automatic sinic, vol. 4, no. 3, Jul. 2017.

[14] J. Liu, Y. Miura and T. Ise, "Comparison of Dynamic Characteristics Between Virtual Synchronous Generator and Droop Control in Inverter-Based Distributed Generators," IEEE Trans. Power Electronics, Vol. 31, no. 5, May 2016.

[15] D. Cheng, Y. Xu, and A. Q. Huang, "Integration of DC Microgrids as Virtual Synchronous Machines Into the AC Grid," IEEE Trans. Industrial Electron. Vol. 64, no. 9, Sep. 2017.

[16] A. Yazdani and R. Iravani, "Voltage-soured Converters in Power Systems," WILEY IEEE PRESS, March 2010, ISBN: 978-0-470-52156-4.pp204-269.

[17] IEC 61400-1, Wind Turbines - Part 1: Design Requirements, International Electrotechnical Commission, Geneva, Switzerland, Tech. Rep. (August 2005).

[18] F. Milano, Power System Modelling and Scripting, Springer, London, August 2010.

[19] F. Milano, A Python-based Software Tool for Power System Analysis, IEEE PES General Meeting, Vancouver, Canada, 21-25 July 2013.

[20] Z. Zeng, R. Zhao, H. Yang, C. Cheng and S. Tang, "Single-Phase Virtual Synchronous Generator for Distributed Energy Sources," 2013 International Conference on Electrical Machines and Systems, Busan, Korea, 26-29, Oct. 2013.

[21] A. Nicastri and A. Nagliero, "Comparison and evaluation of the PLL techniques for the design of the grid-connected inverter systems", 2010 IEEE International Sympoisum on Industrial Electronics (ISIE), Bari, Italiy, 4-7 July 2010.

[22] B. C. Pal, A. H. Coonick, I. M. Jaimoukha, and H. EI-Zobaidi, "A Linear Matrix Inequality Approach to Robust Damping Control Design in Power Systems with Superconducting Magnetic Energy Storage Device," IEEE Trans. Power Systems, vol.15, no.1, pp356-362, Feb. 2000.